WARM ABSORBER, REFLECTION, AND Fe K LINE IN THE X-RAY SPECTRUM OF IC 4329A

M. Cappi,[1] T. Mihara,[1] M. Matsuoka,[1] K. Hayashida,[2] K. A. Weaver,[3] and C. Otani[1]

ABSTRACT

Results from the X-ray spectral analysis of the *ASCA* (*Astro-D*) performance verification (PV) phase observation of the Seyfert 1 galaxy IC 4329A are presented. We find that the 0.4–10 keV spectrum of IC 4329A is best described by the sum of a steep ($\Gamma \sim 1.98$) power-law spectrum passing through a warm absorber plus a strong reflection component and associated Fe K line, confirming recent results (Madejski et al. 1995; Mushotzky et al. 1995). Further cold absorption in excess of the Galactic value and covering the entire source is also required by the data, consistent with the edge-on galactic disk and previous X-ray measurements. The effect of the warm absorber at soft X-ray energies is best parameterized by two absorption edges, one consistent with O VI, O VII, or N VII, the other consistent with O VIII. A description of the soft excess in terms of blackbody emission, as observed in some other Seyfert 1 galaxies, is ruled out by the data. A large amount of reflection is detected in both the gas scintillation imaging spectrometer (GIS) and the solid-state imaging spectrometer (SIS) dectectors, at similar intensities. We find a strong correlation between the amount of reflection and the photon index, but argue that the best solution for the present data is that given by the best statistical fit. The model dependence of the Fe K line parameters is also discussed. Our best fit gives a slightly broad ($\sigma \simeq 0.11 \pm 0.08$ keV) and redshifted ($E \simeq 6.20 \pm 0.07$ keV) Fe K line, with equivalent width (EW) $\simeq 89 \pm 33$ eV. The presence of a weak Fe K line with a strong reflection can be reconciled if one assumes iron underabundances or ionized reflection. We also have modeled the line with a theoretical line profile produced by an accretion disk. This yields results in better agreement with the constraints obtained from the reflection component.

Subject headings: galaxies: individual (IC 4329A) — galaxies: Seyfert — X-rays: galaxies

1. INTRODUCTION

X-ray observations of Seyfert 1 galaxies strongly support the hypothesis that optically thick (column density $\gtrsim 10^{23}$ cm^{-2}) matter surrounds the innermost regions of active galactic nuclei (AGNs) (Nandra & Pounds 1994). The detection of a bump in the continuum emission above ~ 7 keV and an iron fluorescence line at ~ 6.4 keV in several Seyfert galaxies are compelling evidence that the intrinsic continuum is reprocessed by cold matter (Guilbert & Rees 1988; Lightman & White 1988). Recent *ASCA* observations also confirm the existence of ionized matter (the so-called warm absorber) along the line of sight of some Seyfert 1 galaxies (e.g., MCG −6-30-15, Fabian et al. 1994; NGC 3227, Ptak et al. 1994; NGC 3783, George, Turner, & Netzer 1995). In these sources, the warm absorber alone can explain both the absorption features detected around 1 keV and the soft-excess emission. However, this seems not to be the rule for all Seyfert 1 galaxies (Matsuoka 1994). Some of them, like NGC 7469, do not show the presence of ionized absorption but require extra soft emission best characterized by a low-temperature blackbody (Guainazzi et al. 1994). Others, like NGC 4051 and Mrk 766, require both the warm absorber and the blackbody component (Mihara et al. 1994, Leighly et al. 1995; Guainazzi et al. 1995).

In light of these general considerations, the *ASCA* observation of the bright Seyfert 1 galaxy IC 4329A ($z = 0.016$; Wilson & Penston 1979) provides new insights on these issues. From the *Ginga* observation in the 1.7–30 keV energy band, IC 4329A is known to exhibit a strong reflection component which flattens the 1.7–30 keV photon index from an intrinsic value of 1.97 ± 0.04 to the apparent value of 1.71 ± 0.01 (Miyoshi et al. 1988; Piro, Yamauchi, & Matsuoka 1990, hereafter PYM90). The reflection component is accompanied by an iron fluorescence line at $E \sim 6.2$ keV, with an equivalent width (EW) of $\simeq 100 \pm 20$ eV. Evidence of day-to-day ($\sim 50\%$) variations in the amount of reflection relative to the direct continuum have also been reported (Fiore et al. 1992). In the *ROSAT* soft energy band (0.1–2.4 keV), the spectrum of IC 4329A is best described by an absorbed power law with a photon index $\Gamma \simeq 1.83 \pm 0.4$, plus an absorption edge around 0.7 keV having an optical depth of $\simeq 0.6 \pm 0.2$ consistent with absorption by O VI and O VII (Madejski et al. 1995). However, an alternative explanation for the soft excess in terms of a blackbody or a steep power law is also allowed by the same data. All fits derive a column density of a few 10^{21}cm^{-2}. This column density is largely in excess of the Galactic value $N_{\rm H\,gal} \simeq 4.55 \times 10^{20}$ cm^{-2} (Elvis, Lockman, & Wilkes 1989) and indicates absorption intrinsic to IC 4329A. This result is consistent with the fact that its host galaxy is seen edge on (Petre et al. 1984).

In the following, we present the results from the X-ray observation of IC 4329A with *ASCA* (Tanaka, Inoue, & Holt 1994). The data between 2 and 10 keV have been discussed previously in a letter by Mushotzky et al. (1995). We now report a more detailed analysis of the overall (0.4–10 keV) data and show very strong evidence that the X-ray spectrum of IC 4329A is absorbed by highly ionized gas (warm absorber), characterized by the absorption edges of highly ionized oxygen

[1] Institute of Physical and Chemical Research (RIKEN), 2-1, Hirosawa, Wako, Saitama 351-01, Japan.

[2] Department of Physics, Faculty of Science, University of Osaka, 1-1, Machikaneyama-chou, Toyonaka, Osaka 560, Japan.

[3] Department of Astronomy and Astrophysics, 525 Davey Lab, Pensylvania State University, University Park, PA 16802. Presently at Johns Hopkins University, Department of Physics and Astronomy, 3400 North Charles Street, Baltimore, MD 21218.

ions (§ 3.1). We also confirm the presence of a spectral hardening above $\sim 6-7$ keV and the iron K-shell emission line, which are characteristics of a reflection spectrum (§ 3.2). Complex warm absorber models and accretion-disk emission-line models are then discussed (§ 4). We conclude that there is evidence of a warm absorber, a strong reflection component, and a marginally broad iron fluorescence line in the X-ray spectrum of IC 4329A.

2. THE X-RAY DATA

The X-ray observation of IC 4329A reported here was carried out with *ASCA* on 1993 August 15 during the performance verification (PV) phase. Solid-state imaging spectrometer (SIS) daa were collected in four CCD "bright" and "faint" modes. Faint data were converted into bright data. No echo corrections or dark frame error (DFE) corrections were applied (see Otani & Dotani 1994 for details on these effects). Standard selection criteria were used, the most relevant being elevation and bright Earth angles greater than 5° and 25°, respectively, and a magnetic cutoff rigidity greater than 8 GeV/c. These were applied to both the gas scintillation imaging spectrometer (GIS) and the SIS data. The resulting effective exposure times are $\sim 29{,}000$ s for the SIS and $\sim 32{,}500$ s for the GIS. About 55,000 and 90,000 source plus background counts were collected from the SIS and the GIS, respectively. The background count rates were $\sim 1\%$ of the SIS average source count rate (~ 1.7 counts s^{-1}) and about 5% of the GIS average source count rate (~ 2.6 counts s^{-1}).

Only chip 1 of SIS0 and chip 3 of SIS1 were used in the SIS analysis. This results in the loss of $\sim 30\%$ of the total SIS source counts to the neighboring chips due to the broad wings of the mirror point response function. Source counts were extracted from circular regions of radius $\sim 12'$ and $\sim 6'$ for the GIS and the SIS, respectively. Because the source is bright and fills the chip, SIS background was extracted from the SIS blank sky files from the same area as that used for the source. GIS background counts were accumulated from annular regions around the source, with an internal radius of $\sim 14'$ and an external radius of $\sim 17'$. Results with the blank sky GIS backgrounds are consistent with the reported one to within $\sim 5\%$. It has been reported from *ROSAT* observations (Madejski et al. 1995) that two other X-ray sources (the elliptical galaxy IC 4329 and an unidentified source) lie within $\sim 13'$ of IC 4329A. In the following analysis, we will assume that their contribution is negligible since they become important only below ~ 0.5

keV, as pointed out by Madejski ef al. (1995). Neither source is spatially resolved with the SIS or with the GIS, even when we considered only the low energies ($E \lesssim 0.5$ keV) or only the high energies ($E \gtrsim 5$ keV).

Although the source flux decreased by $\sim 15\%$ in a timescale of ~ 1 day in all detectors, a hardness ratio analysis reveals no significant spectral variation during the observation. Therefore, all photons have been accumulated together for the spectral analysis.

3. SPECTRAL ANALYSIS

GIS2/3 and SIS0/1 pulse-height spectra were binned in order to have a number of counts per bin $\gtrsim 200$ and $\gtrsim 100$ in the energy ranges 0.7–10 keV and 0.4–10 keV, respectively. Data preparation and spectral analysis have been performed using version 1.0h of the XSELECT package and version 8.5 of the XSPEC program (Arnaud, Haberl, & Tennant 1991). We made use of the response matrices gisv3_1.rmf (released in 1994 March) for the GIS detectors, and rsp1.1alpha (released in 1994 June) with DFE shifted by -2 analog-to-digital converter units (ADU) (~ 7 eV) and -5 ADU (~ 18 eV) for the SIS0 and SIS1 detectors, respectively.

For the GIS data, we first modeled the overall 0.7–10 keV spectrum with a single absorbed power law plus iron emission line. The column density, $N_{\rm H}$, was free to vary. This model gives an acceptable ($\chi^2_{\rm red}$/degrees of freedom [dof] $\simeq 1.33/564$) description of the spectrum with $\Gamma \simeq 1.79 \pm 0.02$, a column density $N_{\rm H} \simeq (3.8 \pm 0.2) \times 10^{21}$ cm^{-2}, and a very broad ($\sigma \simeq 0.53 \pm 0.24$ keV) iron emission line at $E \simeq 6.19 \pm 0.15$ keV with EW $\simeq 233 \pm 80$ eV (see Table 1A). With these values, the unabsorbed flux in the 2–10 keV energy band is $\simeq 1.01 \times 10^{-10}$ ergs cm^{-2} s^{-1}, which corresponds to a luminosity $L_{2-10\,{\rm keV}} \sim 1.07 \times 10^{44}$ ergs s^{-1}. Although the continuum shape is approximately consistent with previous measurements with the same model (PYM90; Madejski et al. 1995), the iron line appears much broader and a factor of ~ 2 stronger than previous values (PYM90; Nandra & Pounds 1994). However, this difference can be easily understood if we consider that, as shown later on, the SIS data strongly require the addition of a reflection component to the continuum emission (§ 3.2). Because of its better resolution, the SIS can indeed better separate the Fe K line from the reflection component. When the reflection is included in the model, the Fe K line parameters obtained from the GIS data are considerably reduced (Table 1B) and become consistent with *Ginga* and the

TABLE 1
GIS2 + 3 DATA (0.7–10 KEV)
A. RESULTS OF POWER LAW + Fe K LINE FITS

$N_{\rm H}$ (10^{21} cm^{-2})	Γ	$A_{\rm pl}$[a]	E(Fe K) (keV)	σ(Fe K) (keV)	EW(Fe K) (eV)	$\chi^2_{\rm red}$/dof
$3.78^{+0.18}_{-0.12}$	$1.79^{+0.02}_{-0.03}$	$27.6^{+0.7}_{-0.7}$	$6.19^{+0.12}_{-0.15}$	$0.53^{+0.24}_{-0.24}$	233^{+95}_{-73}	1.33/564

B. RESULTS OF POWER LAW + Fe K LINE + REFLECTION FITS

$N_{\rm H}$ (10^{21} cm^{-2})	Γ	$A_{\rm refl}$[a]	R[b]	E(Fe K) (keV)	σ(Fe K) (keV)	EW(Fe K) (eV)	$X^2_{\rm red}$/dof
$4.22^{+0.24}_{-0.27}$	$1.89^{+0.05}_{-0.04}$	73^{+28}_{-28}	$2.43^{+1.04}_{-0.95}$	$6.22^{+0.08}_{-0.08}$	$\lesssim 0.26$	78^{+38}_{-24}	1.30/563

NOTE.—Intervals are at 90% confidence for one interesting parameter.
[a] Normalization in 10^{-3} photons cm^{-2} s^{-1} keV^{-1} at 1 keV.
[b] $R \equiv A_{\rm refl}/A_{\rm pl}$ (see § 3.2 for details).

SIS results. A detailed description of the reflection parameters given in Table 1B, as well as the full justification for the use of this model, is presented in § 3.2, in the light of the results obtained from the SIS spectrum.

For the SIS data, a single absorbed power-law model with $N_H \sim 4 \times 10^{21}$ cm^{-2} and $\Gamma \sim 1.75$ gives an unacceptable fit, with χ^2_{red}/dof $\simeq 2.21/551$. The residuals to this fit between 0.4 and 10 keV are shown in Figure 1 and are indicative of the complexity of the X-ray spectrum of IC 4329A. At low energies, the residuals show the presence of excess emission at $E \lesssim 0.8$ keV and absorption features around 1 keV. These indicate that either the underlying soft continuum emission is more complex than a single power law, or the absorption is more complex than a uniform, cold absorption. At higher energies, we find an Fe K emission line at $E \sim 6.2$ keV but also systematic positive residuals starting from $E \gtrsim 5$ keV. The presence of this "hard tail" will appear more evident (§ 3.1.2) after fitting adequately the low-energy part of the spectrum.

Because of the complexity of the SIS spectrum, we split the following analysis into two parts: (1) fit of the spectrum between 0.4 and 5 keV in order to focus only into the characteristics of the low-energy band, and (2) fit of the overall (0.4–10 keV) spectrum.

3.1. Low Energy Band

3.1.1. Thermal Component

One possibility to explain the measured soft excess would be to assume a two-component continuum emission instead of a single power law. A steep, ultrasoft excess may be associated with emission from the inner parts of an accretion disk (Wilkes & Elvis 1987; Turner & Pounds 1989). As a first approximation, this soft emission can be parameterized by a low-temperature ($T \lesssim 10^6$ K, $kT \lesssim 100$ eV) blackbody. A model consisting of a blackbody plus absorbed power law was fitted to the 0.4–5 keV SIS spectrum (SIS0 and SIS1 are fitted simultaneously). The resulting blackbody temperature of $\sim 9.3 \times 10^5$ K ($kT \sim 80$ eV), photon index of ~ 1.96, and column density of $\sim 5.8 \times 10^{21}$ cm^{-2} are consistent with previous ROSAT results (Madejski et al. 1995), but the residuals shown in Figure 2a present strong and systematic deviations around $E \simeq 0.6$ keV and absorption features around 0.9 keV. These clearly indicate that the blackbody model, alone, cannot explain the measured soft excess. The further addition of an absorption edge at $E \sim 0.76$ keV with $\tau \sim 0.46$ improves the statistics of the fit to χ^2_{red}/dof $\simeq 1.22/481$. In that case, the normalization of the blackbody is reduced by a factor of ~ 5, and some systematic structures are still present in the residuals around 0.9 keV. These also imply that this possibility is unlikely.

Alternatively, we modeled the soft excess with a Raymond-Smith plasma model (Raymond & Smith 1986) absorbed by the Galactic column only. This model has been proposed in the past as a possible explanation for the soft excess observed in some Seyfert 1 galaxies (Turner et al. 1991). The best result is obtained by allowing the abundances to be free. This gives a plasma temperature of $\sim 2.1 \times 10^6$ K ($kT \sim 183$ eV) and improves the fit to χ^2_{red}/dof $\simeq 1.28/479$. However, the best-fit abundances are $\sim 1/20$ the solar value. Such a required low abundance is obvious from the absence of any blend of emis-
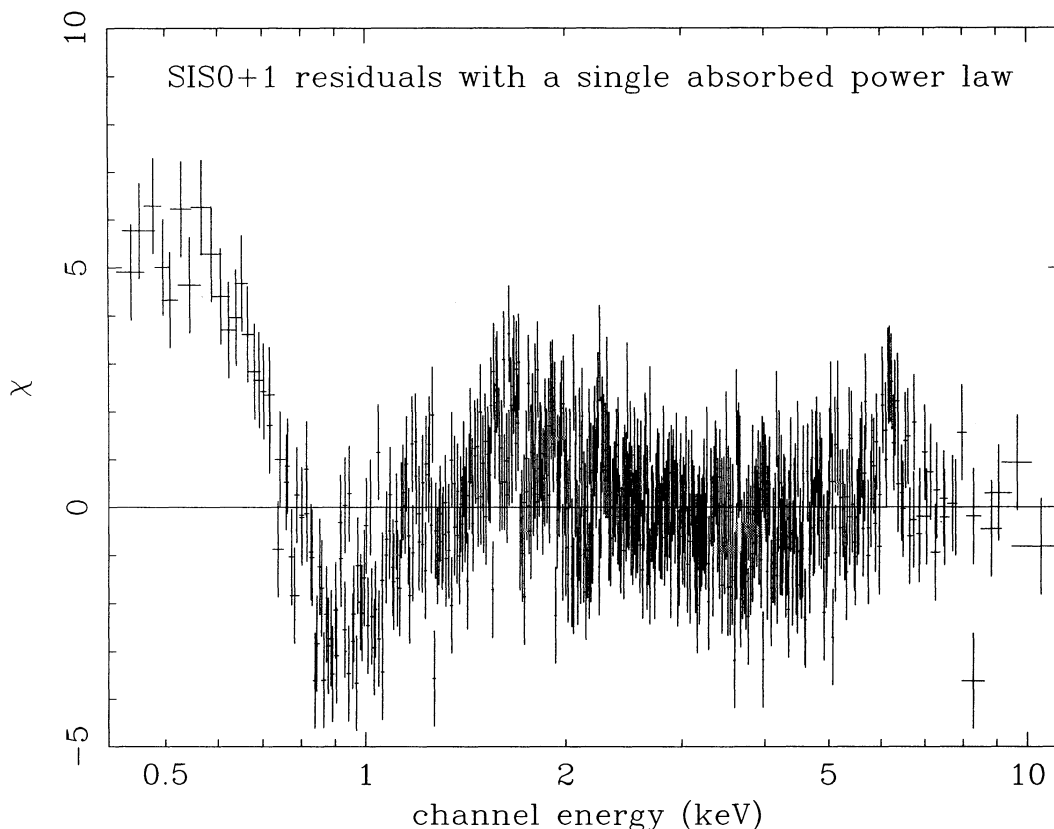

FIG. 1.—Residuals of the SI spectrum between 0.4 and 10 keV for a model consisting of a single absorbed power law with $\Gamma \sim 1.75$. This figure illustrates the soft excess, absorption features around 1 keV, Fe K line at ~ 6.2 keV, and hard tail starting at $E \gtrsim 5$ keV (see also Fig. 5).
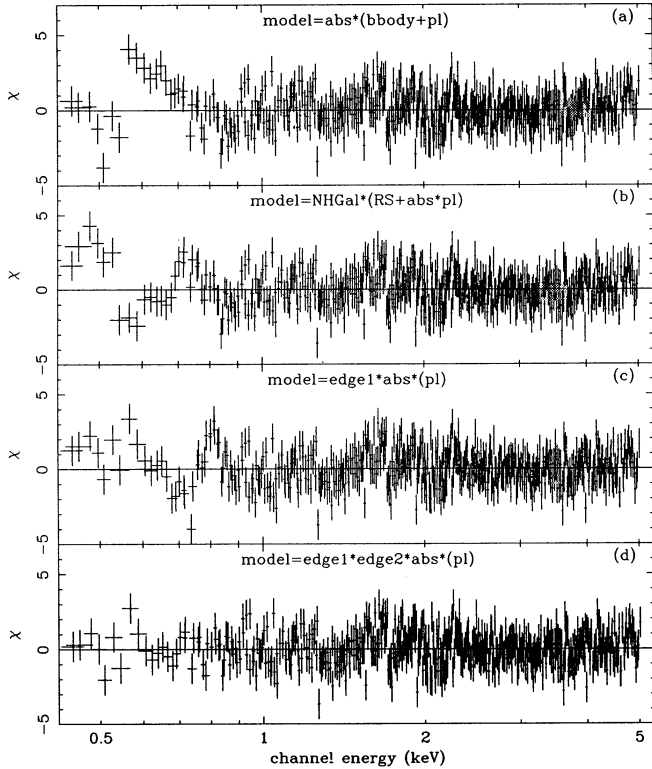
FIG. 2.—Residuals of the SIS spectrum between 0.4 and 5 keV for a model consisting of: (a) absorbed blackbody plus power law, (b) absorbed power law plus Raymond-Smith spectrum covered by only the Galactic column density, (c) absorption edge plus absorbed power law, and (d) two absorption edges plus absorbed power law.

sion lines around 0.8–0.9 keV. Moreover, some systematic features are present in the residuals (Fig. 2b). Thus, we also exclude this alternative as a possible description of the soft X-ray spectrum of IC 4329A.

3.1.2. *Absorption Edges*

Another possible explanation for the soft excess is an ionized or "warm" absorber. The ionized absorber model assumes that light elements (O, Ne, Mg, Si, and Fe) are photoionized and therefore predicts extra emission due to the reduction of the opacity at low energies. This model also predicts extra absorption around 1 keV, mainly due to highly ionized oxygen (Netzer 1993). It is clear from the residuals shown in Figure 1 that both these features are detected in the spectrum of IC 4329A. These strongly support, a priori, the ionized absorber model.

As a first approximation of a warm absorber, we added a single absorption edge to the absorbed power-law model. Given the good statistics of the present data ($\sim 50,000$ counts/SIS) and the *ASCA* spectral resolution (FWHM ~ 80 eV at 1 keV), a single absorption edge is a rather crude approximation

of a warm absorber, but it allows a direct comparison with previous measurements. The inclusion of an absorption edge in the absorbed power-law model improves the fit to $\chi^2_{red}/dof \simeq 1.30/479$, and gives $E_{edge} \simeq 0.76 \pm 0.01$ keV and $\tau_{edge} \simeq 0.84 \pm 0.04$. These values are consistent with the *ROSAT* results (Madejski et al. 1995). However, inspection of the residuals in Figure 2c clearly suggests further complexity. Indeed, the addition of a second absorption edge improves the statistics to $\chi^2_{red}/dof \simeq 1.15/477$, which is significant at more than a 99.9% level ($\Delta\chi^2 \simeq 76$). As evident from the residuals in Figure 2d, the two edges plus absorbed power-law model provide the best description of the soft X-ray spectrum. Best-fit parameters are reported in Table 2, and confidence contours for the edge energies versus optical depths are shown in Figure 3. Assuming a conservative value of ~ 10 eV (1σ) for the SIS systematic uncertainties, the edge at $E \simeq 0.70 \pm 0.02$ keV is consistent with absorption by O VI (671 eV), O VII (739 eV), and N VII (667 eV), where the energies quoted in parentheses are the edge energies in the rest frame (Lotz 1968). The best agreement is the O VII. The second edge at $E \simeq 0.84 \pm 0.02$ keV is consistent with O VIII (871 eV) only. Inspection of the residuals in Figure 4 shows the presence of a further edgelike feature at ~ 1.25 keV, consistent with Ne IX (1196 eV), Ne X (1362 eV), and Fe L edges of Fe ionization stages around Fe XVIII. Inclusion of a third absorption edge in the model, however, is significant only at a $\sim 68\%$ confidence level. Given its low statistical significance, we do not consider it further. It is interesting to note that both characteristic energies obtained for the O VII and O VIII edges are redshifted by approximately the same amount (~ 25 eV, in the observer frame). We checked that this redshift is not related to the charge transfer inefficiency (CTI) of the SIS (see Otani & Dotani 1994 for details).

Because IC 4329A is a fairly bright point source, we may expect any systematic problems due to remaining calibration uncertainties to be more visible in IC 4329A than in other, weaker sources. We point out that some features are present between ~ 1.8 and 2.5 keV. These are likely to be due to calibration uncertainties in this energy range (Si K edge and Au M edge of the detector). In this work, we will assume that these features are not of cosmic origin and are therefore of no physical interest.

Also, even after applying our best-fit edge model (above), there are still residuals in the shape of an emission line around 0.6 keV and an absorption feature around 0.5 keV. In particular, the emission line can be fitted with a narrow ($\sigma \equiv 0$) Gaussian line at $E \simeq 0.58 \pm 0.05$ keV with EW $\simeq 30 \pm 25$ eV. The inclusion of this emission line corresponds to a $\Delta\chi^2 \sim 4$, which is significant at more than 95% confidence. Its energy is consistent with emission from O VII and/or O VIII. The existence of similar emission lines is predicted in warm absorber models (Netzer 1993) and has been confirmed in the Seyfert 1 galaxy NGC 3783 (George et al. 1995). However, it is also known from other *ASCA* observations that features around 0.5–0.6 keV are very sensitive to calibration uncertainties (due to the O K edge

TABLE 2

SIS0 + 1 DATA (0.4–5 keV): RESULTS OF TWO EDGES + POWER-LAW FITS

E_1 (eV)	τ_1	E_2 (keV)	τ_2	N_H (10^{21} cm^{-2})	Γ	A_{pl}[a]	χ^2_{red}/dof
$0.70^{+0.01}_{-0.03}$	$0.63^{+0.09}_{-0.08}$	$0.84^{+0.01}_{-0.02}$	$0.39^{+0.06}_{-0.07}$	$3.30^{+0.08}_{-0.09}$	$1.89^{+0.03}_{-0.03}$	$29.5^{+0.7}_{-0.7}$	1.15/477

NOTE.—Intervals are at 90% confidence for one interesting parameter.

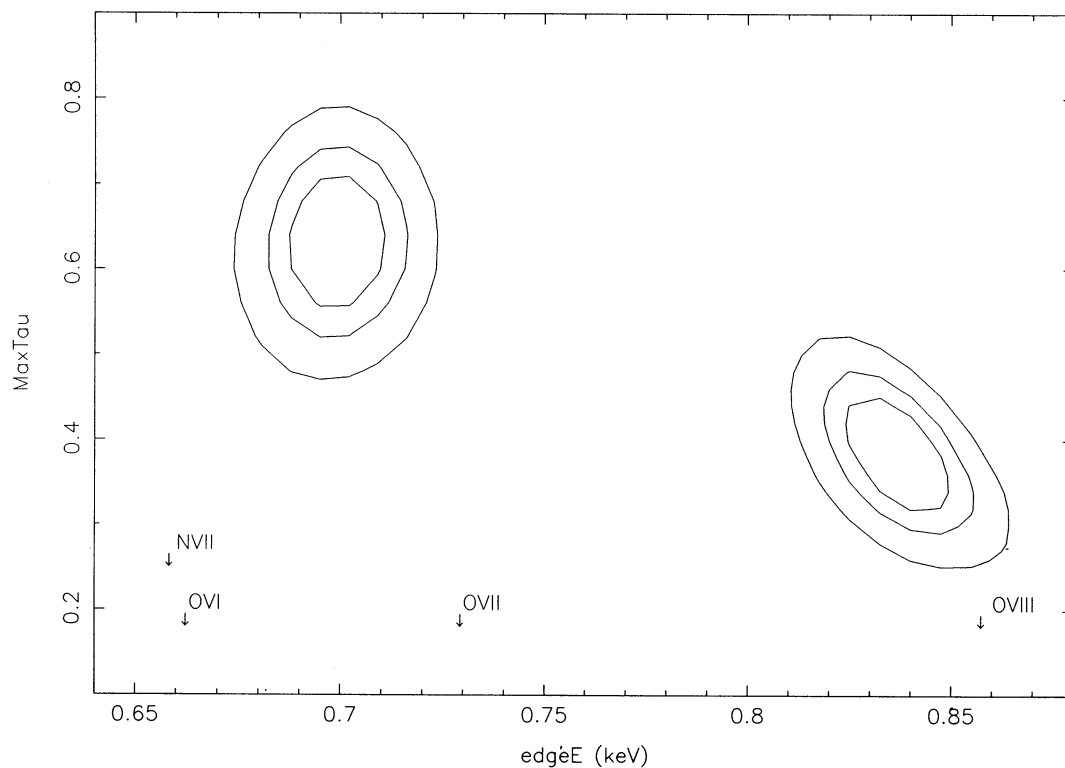[a] Normalization in 10^{-3} photons cm^{-2} s^{-1} keV^{-1} at 1 keV.

FIG. 3.—Contour plots illustrating the (observed) energy and optical depth at 68%, 90%, and 99% confidence levels of the two absorption edges at $E \sim 0.7$ keV and $E \sim 0.84$ keV. The redshifted energies of the absorption edges have been marked in the figure.
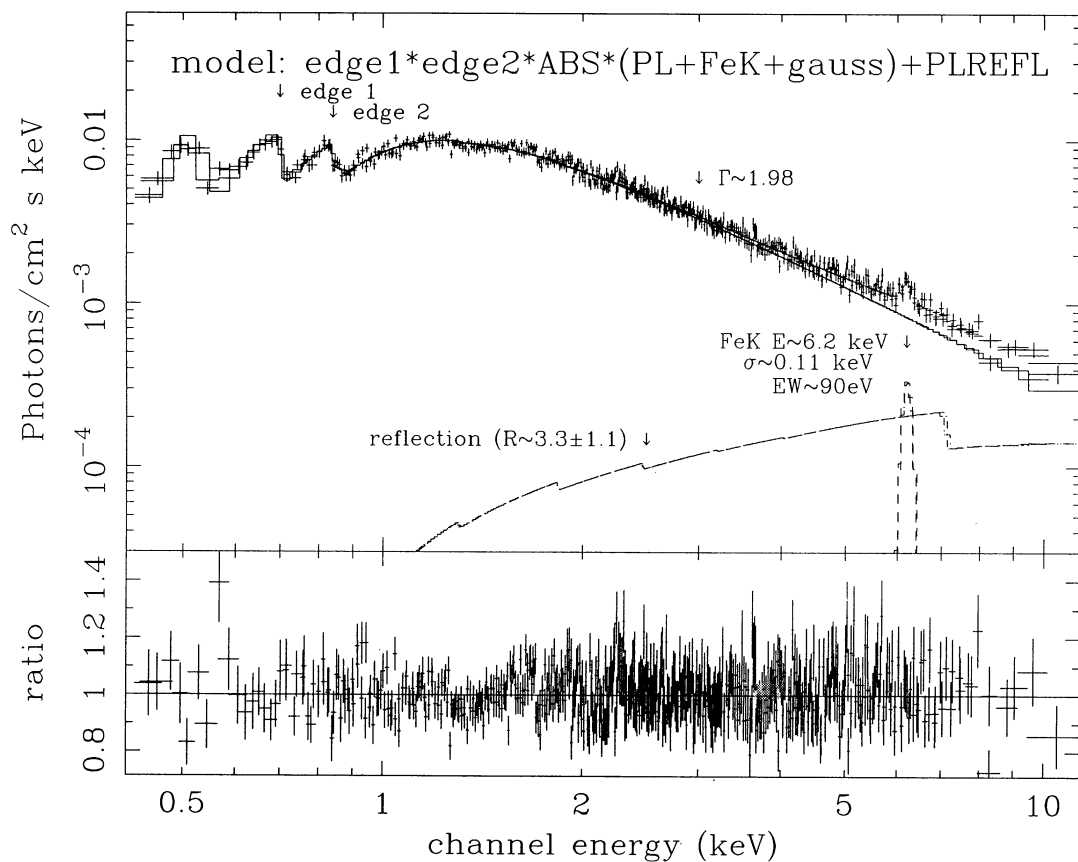

FIG. 4.—SIS0 + 1 unfolded spectrum, best-fitting power law plus two absorption edges plus Fe K line plus reflection model (*upper panel*). Residuals in the form of the ratio data model are shown in the lower panel.

at ∼0.54 keV), background subtraction, and selection criteria (Miura et al. 1995). Therefore, we have carefully checked to establish the believability of this soft emission line.

When different background regions are used and different selection criteria (like bright Earth angle > 50, for example) are applied, both the absorption and soft emission line features remain unchanged. Using the "gain" command in XSPEC, we (linearly) shifted the energies of the SIS0 and SIS1 response matrices by ±2 ADU (∼7 eV), i.e., within typical systematic errors of ∼10 eV (1 σ) for the DFE "zero level" (Otani & Dotani 1994). After fitting the data again with the shifted matrices, the absorption feature around 0.5 keV appears smoothed out. It is therefore probably due to calibration uncertainties. While the soft emission line changes in intensity, it remains statistically significant in every case. However, the emission line is significant only in the SIS1 data. Also, it appears to go away when only the night data are considered, although, in this case, the statistics are considerably reduced. We conclude that with the present data, the existence of this emission line is doubtful.

3.2. *Overall Spectrum*

We now also include the data from $E > 5$ keV and proceed to the analysis of the spectrum in the broad (0.4–10 keV) energy band. One striking result is that we detect a clear hardening of the spectrum even down to 5–6 keV, likely due to the presence of a reflection component, as previously found by Mushotzky et al. (1995). Figure 5 illustrates the existence of the hard tail and a Fe K emission line around 6.2 keV. To produce

this figure, the spectrum was fitted between 0.4 and 5 keV with the two edges plus power law model (§ 3.1.2, Table 2), and the data above 5 keV were added back in. The data were rebinned to more than 500 counts bin^{-1} in order to show better the presence of the hard tail. The systematic positive values of the residuals, before and after the Fe K emission line, are a clear indication that the continuum is increasing at higher energies. This is also confirmed by the huge ($\sigma \sim 1.17$ keV and EW ~ 760 eV) values obtained for the Fe K line ($E \sim 6.25$ keV) if we include only a single Gaussian line in the model, which tries to account for the line plus the hard tail. We underline that in this case, as well as in all the following spectral fits, all the parameters of the two edges plus power law in the model are free. Given the importance of the residuals above 7 keV, we carried out a number of tests to confirm the reality of the hard tail. The use of a background chosen from the outer region of the relevant chip in the SIS had no significant effect on either the overall spectrum or the strength of the hard tail. The use of different extraction radii for the source (from $r = 4'$ to $r = 9'$) and more conservative selection criteria (like bright Earth angle > 50 to avoid light leakage) gave similar results as well.

In a recent *ASCA* long observation of the Seyfert 1 galaxy MCG −6-30-15, a very broad iron line has been observed (Tanaka et al. 1995). It has been well modeled by the sum of a broad ($E \sim 5.6$ keV, $\sigma \sim 0.64$ keV, and EW ~ 120 eV) and a narrow ($E \sim 6.4$ keV, $\sigma \sim 0.20$ keV, and EW ~ 200 eV) Gaussian lines. These have been interpreted as the signature of the "double-horned" line expected from an accretion disk (e.g., Fabian et al. 1989). If a double-Gaussian parameterization is used for IC 4329A instead of a single line, one Gaussian con-
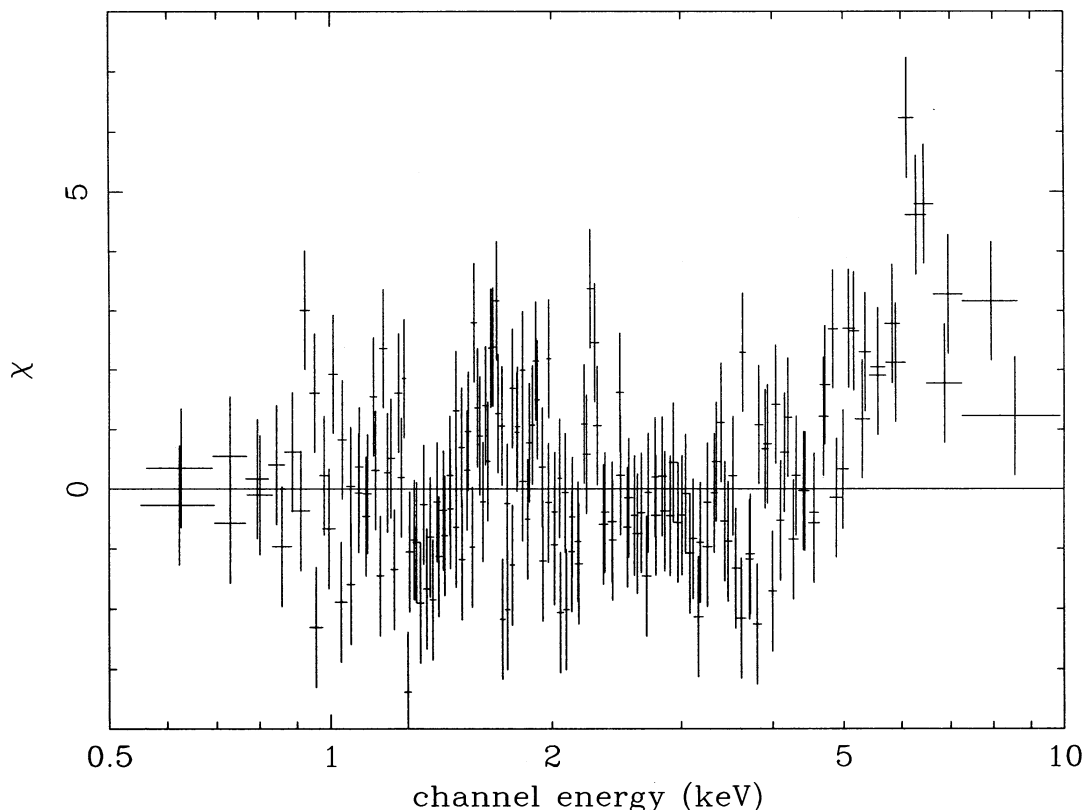

FIG. 5.—Residuals of the SIS spectrum between 0.4 and 10 keV for a model consisting of two absorption edges plus an absorbed power law fitted between 0.4 and 5 keV. The data have been rebinned with more than 500 counts bin^{-1} to show better the systematic increase of the residuals above 5 keV.

TABLE 3

SIS0 + 1 DATA (0.4–10 KEV): RESULTS OF TWO EDGES + POWER LAW + Fe K LINE + REFLECTION FITS

E_1 (keV)	τ_1	E_2 (keV)	τ_2	N_H (10^{21} cm^{-2})	Γ	A_{refl} [a]	R [b]	E(Fe K) (keV)	σ(Fe K) (keV)	EW(Fe K) (eV)	χ^2_{red}/dof
$0.70^{+0.01}_{-0.02}$	$0.67^{+0.07}_{-0.09}$	$0.84^{+0.01}_{-0.02}$	$0.40^{+0.07}_{-0.07}$	$3.48^{+0.12}_{-0.13}$	$1.98^{+0.05}_{-0.05}$	102^{+41}_{-34}	$3.35^{+1.17}_{-1.10}$	$6.20^{+0.07}_{-0.06}$	$0.11^{+0.07}_{-0.09}$	89^{+34}_{-32}	1.15/546

NOTE.—Intervals are at 90% confidence for one interesting parameter.

[a] Normalization in 10^{-3} photons cm^{-2} s^{-1} keV^{-1} at 1 keV.

[b] $R \equiv A_{refl}/A_{pl}$ (see § 3.2 for details).

verges to a very broad ($\sigma \sim 1.2$ keV and EW ~ 713 eV) line centered at 6.2 keV and the other to a narrow ($\sigma = 0$ and EW ~ 53 eV) line at the same energy. Since the data require an unusually broad Gaussian that is nonphysical and inconsistent with any previous X-ray measurement, we prefer to interpret this result to mean that the high-energy part of the spectrum requires an additional continuum component.

The presence of a Fe K emission line and a hard tail is usually interpreted in terms of a model in which the primary continuum emission is reprocessed by optically thick matter, i.e., a reflection component (Lightman & White 1988; Nandra & Pounds 1994). Therefore, we added a reflection component in the two edges plus power-law model. A Gaussian emission line is also included in the fit. The reflection used is the "plrefl" model in XSPEC and is calculated following Lightman & White (1988). The reflecting matter is assumed to be thick, cold, and with cosmic abundances (Morrison and McCammon 1983). The inclination angle i has been fixed to zero, i.e., the reflecting plane is seen face-on, and the covering factor $\Omega/2\pi$ has been fixed to unity. The source is assumed to emit isotropically, and the spectrum is integrated over all viewing angles. The relative normalization $R(\equiv A_{refl}/A_{pl})$ between the

reflected component (A_{refl}) and the direct component (A_{pl}) is a free parameter. This implies that the normalization of the reflection component is allowed to be independent of the normalization of the power law. The parameter R, alone, includes the uncertainties concerning the geometry of the reflector (i.e., the covering fraction), the possibility that the source is anisotropic (e.g., Ghisellini et al. 1991), and time-lag effects. This implies, for example, that a best-fit value of $R \sim 1$ can be explained if the reprocessing material covers $\sim 2\pi$ of the source. If $R > 2$, then the result cannot be explained *only* in terms of a covering factor increase, and either the source must be anisotropic or there are time-delay effects.

The photon index has been left free to vary. The best-fitting parameters with a reflection fit are given in Table 3. The unfolded spectrum and residuals are shown in Figure 4. The measured photon index of 1.98 ± 0.05, $N_H \simeq (3.48 \pm 0.12) \times 10^{21}$ cm^{-2}, and Fe K line parameters ($E \simeq 6.20 \pm 0.07$ keV, $\sigma \simeq 0.11 \pm 0.08$ keV, and EW $\simeq 89 \pm 33$ eV) are consistent with previous *Ginga* results (PYM90; Fiore et al. 1992). Confidence contours in the Fe K parameter space σ-E are well constrained (Fig. 6). These show that the Fe K line is consistent with redshifted cold iron at more than a 90% confidence level
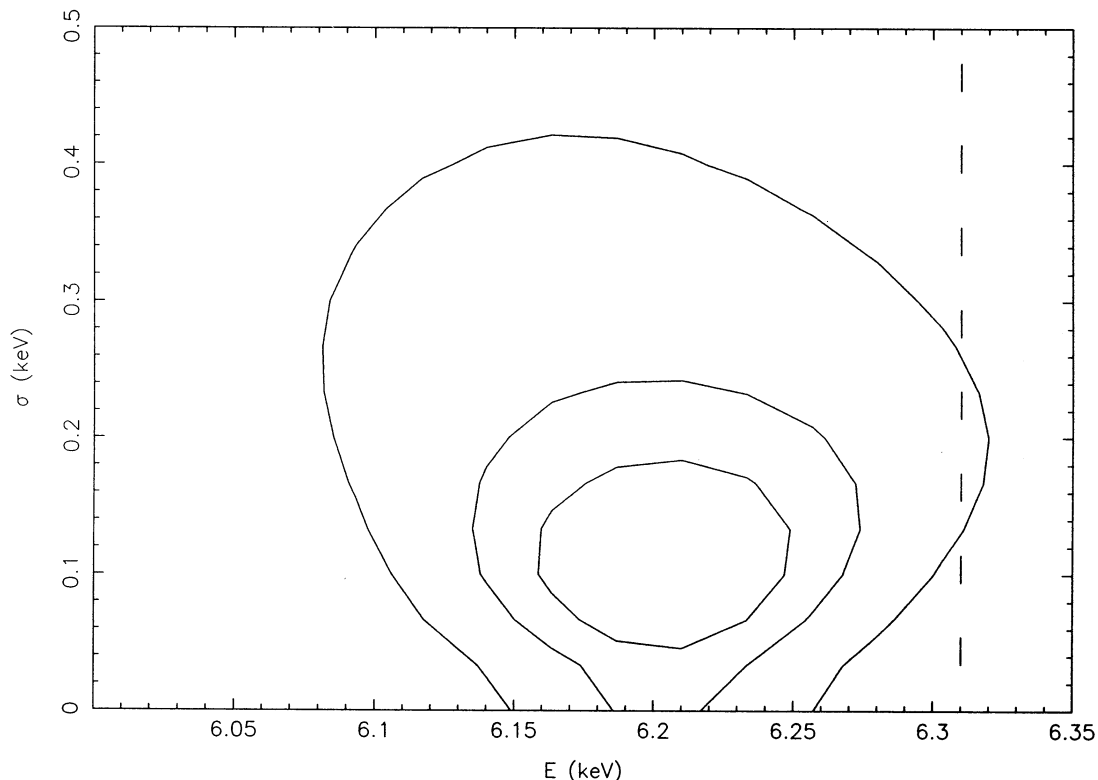

FIG. 6.—Fe K width and energy at 68%, 90%, and 99% confidence contour levels for the best-fit model, as given in Table 3

and is marginally broad at an $\sim 80\%$ confidence level. As discussed later on, these characteristics of the iron line suggest that we are dealing with a disk geometry (Fabian et al. 1989; Mushotsky et al. 1995).

As already mentioned in § 3, the GIS spectral analysis is completely consistent with that derived above for the SIS data. In fact, the inclusion of a reflection component, assuming an inclination $i = 0$ and a covering factor $\Omega/2\pi = 1$ as for the SIS spectrum, improves the GIS fit at a confidence level greater than 99% ($\Delta\chi^2 \sim 21$). Comparison of the GIS best-fit parameters (Table 1B) with those obtained from the SIS data (Table 3) shows very good agreement from both detectors and allows us to be fairly confident in the proposed best-fitting model. The major discrepancies are in the N_H and photon index best-fit values, which are respectively higher and flatter in the GIS than in the SIS spectrum. However, these differences are likely attributable to the fact that the GIS is not sensitive enough at low energies to detect the absorption edges. Since they are not fitted explicitly in the GIS spectrum, they likely enhance the absorption value and therefore contribute to the flattening of the GIS spectrum. This hypothesis is also supported by the fact that the fit of the spectrum with all four detectors (SIS + GIS) gives results almost identical to that found only with the SIS.

3.3. On the Model-dependence of Photon Index, Reflection Normalization, and Fe K Line Parameters

With the above best statistical fit of IC 4329A (Table 3), we found that there is a strong (linear) correlation between the photon index and the amount of reflection (Fig. 7). This relation should be borne in mind when interpreting the results of this analysis. A similar effect has been discussed for the analysis of MCG -2-58-22 (Weaver et al. 1995). While a high best-fit value of R may indeed indicate that the true intrinsic photon

index is steep, it also depends strongly on fitting the correct amount of reflection, as well as the shape of the reflected spectrum modeled. There is no guarantee that the current reflection model is entirely correct, and we may bias the fits with a slightly incorrect shape or normalization of the reflection. Different analysis procedures may, therefore, lead to slightly different results. For example, fixing the photon index to its 90% upper limit ($\Gamma \simeq 1.92$) obtained from the fit in the 0.4–5 keV energy band (Table 2), the amount of reflection converges to $R \simeq 2.1$. However, fixing the photon index from the fit at low energies is not necessarily correct in this case, because we may also bias our fit with an improper parameterization of the warm absorber. Alternatively, fixing $R = 1$, a value appropriate for a face-on slab subtending a 2π solid angle at the X-ray source, the fit gives $\Gamma \simeq 1.89$. However, again in this case, there is no reason to fix R. Therefore, the best solution with the present data is that obtained with Γ and R free to vary (Table 3).

Because of the correlation between photon index and the amount of reflection in the model, we investigated how much this could affect the parameters obtained for the Fe K line. For this, we calculated the 90% confidence contours of σ versus energy for Fe K, with R varying from zero (no reflection) to 3.35 (the best-fit value). These contours are shown in Figure 8 for $R = 0, 0.3, 1, 1.5, 2.1$, and 3.35. The corresponding best-fit values of the Fe K line width are 1.17, 0.89, 0.21, 0.15, 0.13, and 0.11 keV, respectively. The χ^2 values are 641, 640, 639, 634, 630, and 626 for 547 dof. We see that the energy of the Fe K line depends only slightly on the exact amount of reflection. These contours are indicative of three different "solutions" for the line width: (1) assuming little or no reflection ($R \lesssim 0.9$) results in a very broad Fe K line with characteristic width $\gtrsim 0.8$ keV and EW $\gtrsim 380$ eV; (2) assuming an intermediate contribution from reflection ($R \sim 1$–2) results in two local minima, one near $\sigma \sim 0.6$–0.8 keV and the other near $\sigma \sim 0.1$–0.2 keV; and (3)
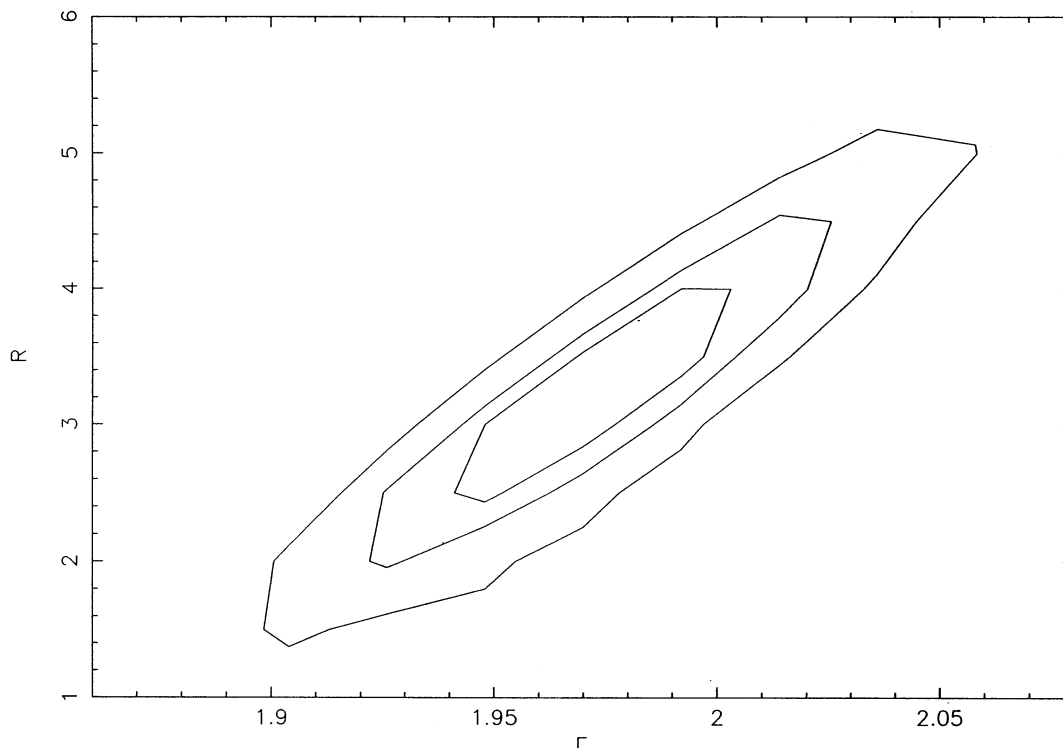

Fig. 7.—Contours at 68%, 90%, and 99% confidence of amount of reflection (R) vs. photon index (Γ). They illustrate the strong correlation between the two parameters.
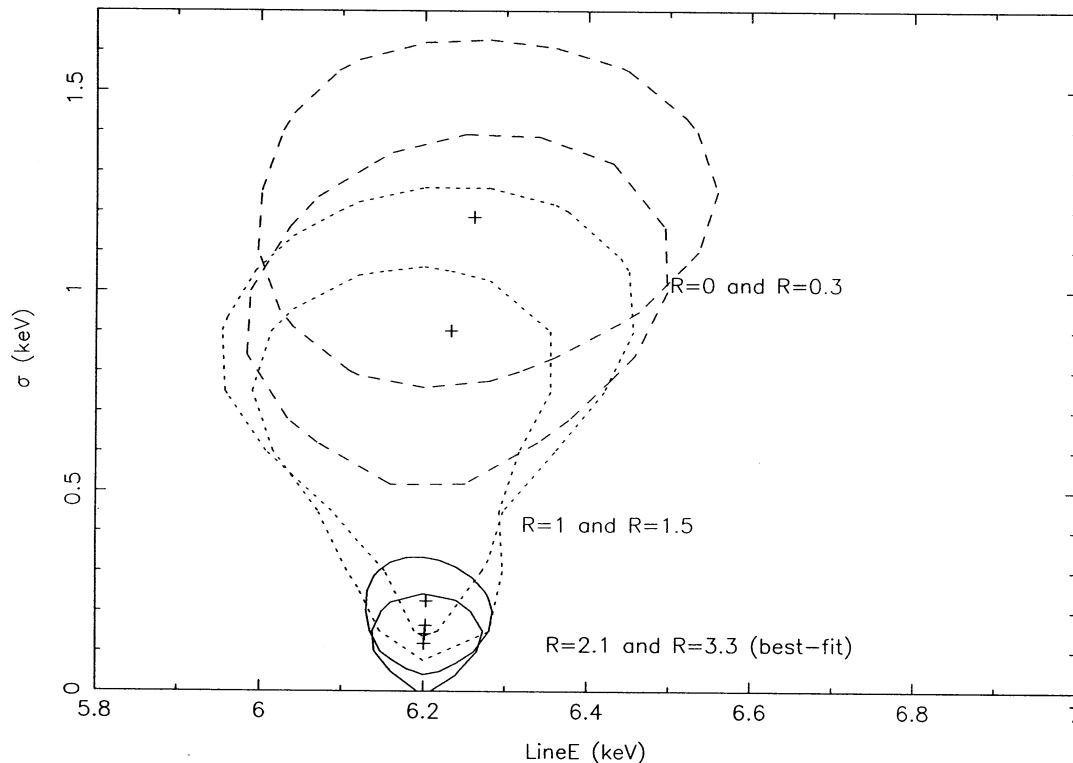
FIG. 8.—Contours at 90% confidence of amount of line width, σ, vs. observed line energy calculated for various amounts of reflection. The best-fit values are marked with crosses.

assuming a strong reflection component (R from ~ 2 to the best-fit value of ~ 3.3) results in one minimum at $\sigma \sim 0.11$ keV with well-constrained contours. Simultaneously fitting the 2 SIS and 2 GIS detectors yielded very similar results. These contours, as well as the best-fit values, are similar to those obtained by Mushotzky et al. (1995), although their fit yields a slightly larger Fe K width than inferred from our best fit (solution 3). The difference may be a consequence of the slightly different continuum modeling, probably caused by the different energy band used by the authors.

To summarize, we find that, although the photon index and reflection normalization are strongly coupled together, the most likely description of the spectrum of IC 4329A is given by its best statistical fit (Table 3). We have also shown that, despite this intrinsic uncertainty, the Fe K parameters depend very little on the exact amount of reflection, provided R is higher than ~ 2, as required by the best-fit model. With these caveats in mind, we can try to interpret these results physically.

4. DISCUSSION

The above results show that the best interpretation of the soft X-ray spectrum of IC 4329A is in terms of a photoionized absorber. Therefore, we have also fitted the SIS data between 0.4 and 5 keV with a warm absorber model, which also included a uniform cold absorber. The model has been produced using the photoionization code CLOUDY (Ferland 1991) and the assumptions in Fabian et al. (1994). Free parameters are the ionization parameter $\xi = L/nR^2$ (ergs s^{-1} cm), the "warm" column density N_W (cm^{-2}), and the cold column density N_H (cm^{-2}). The photon index has been fixed to 2.0, a value close to the SIS best-fit value. The fit yields an acceptable fit with $\chi^2_{red}/dof = 1.23/480$. Although it is a statistically better

fit than that with the blackbody model, it is a worse fit than that with the two absorption edges. We attribute this difference to the fact that the model used is based on simple basic assumptions which may not reflect the reality, namely: a thin geometry for the photoionized gas, solar abundances, constant temperature, constant density, and a source luminosity of 10^{43} ergs s^{-1}. Further, the model does not include the emission lines expected from a more realistic warm absorber (Netzer 1993). We obtain log $\xi \simeq 1.12 \pm 0.04$, log $N_W \simeq 21.70 \pm 0.02$, and log $N_H \simeq 21.49 \pm 0.01$. The fitted neutral column density is again ~ 1 order of magnitude higher than the Galactic value.

It is interesting to note that with the two-edge parameterization of the warm absorber, both of the edges' best-fit energies are redshifted by approximately 25 eV. If this is real, this redshift corresponds to a Doppler velocity of $\sim 10,000$ km s^{-1}. Although this result depends strongly on the correct modeling of the warm absorber (e.g., the redshift of the lower edge may be interpreted as a blend of O VI and O VII edges) and on the precise calibration of the energy scale, it may be the signature of infalling matter or large-scale turbulence associated with the warm absorber region. Firm conclusions on this point require more investigations, but we point out that edge energies, shifted compared to their expected energy, have also been reported for the observations of MCG -6-30-15 and NGC 4051 (Otani 1995).

As suggested by Krolik & Kriss (1995), resonance-line scattering may contribute significantly to the total opacity of the warm gas. It is worth noting, therefore, that it is a potentially confusing factor when interpreting the energy and optical depth of the absorption edges. For example, the presence of blended resonance oxygen lines may cause a misidentification of O VIII as O VII due to the apparent energy shift at the onset

of the O VIII edge. Alternatively, it could contribute to the shift in the apparent energies of the absorption edges. Unfortunately, given that quantitative considerations on resonance absorption are strongly model-dependent (e.g., on the covering factor and velocity of the warm gas), and given the limited spectral resolution of the SIS, we cannot exclude the presence of resonance absorption lines in the present data.

A striking alternative to the warm (plus cold) absorber is absorption by cold matter with abundances free to vary. IC 4329A is known to exhibit absorption of a few 10^{21} cm^{-2}. This absorption is consistent with the fact that its host galaxy is seen edge-on, and so we examine whether the absorption edges seen in the $ASCA$ data can be the result of neutral interstellar matter. Since the K-edge energies of O VII, O VIII, and Ne X are close to the L-edge energy of Fe I, and the K-edge energies of Ne I and Mg I, respectively, it is possible that abundances larger than the cosmic value can mimic the absorption edges normally interpreted as the presence of a warm absorber. In fact, a fit of the low energy band (0.4–5 keV) with a cold absorber with variable abundances gives an equally good fit as that obtained with our previous parameterization using two warm edges (§ 3.1.2). However, extremely high abundances (~ 5–15 times the cosmic value) of all metals are required. Also, known calibration problems around 0.5–0.6 keV (see § 3.1.2) make the results from this fit doubtful. A deeper investigation using these and other data is currently being conducted and will be presented in a future paper (Hayashida et al. 1995, in preparation).

The X-ray spectrum of IC 4329A also requires a remarkably strong reflection component. In a recent reanalysis of $HEAO$ 1 (2–40 keV) data, a similar amount ($R \sim 2.3$–4.2) of reflection component has been detected in IC 4329A (Weaver, Arnaud, & Mushotzky 1995). Similarly, we find in the $ASCA$ spectra ~ 2–3 times more reflection relative to the continuum than in the $Ginga$ observation (PYM90; Fiore et al. 1992; Nandra & Pounds 1994). The present data also suggest a slight, but significant, increase in the absolute amount of reflection. Although we might recall that the $ASCA$ best-fit spectra, as well as the $HEAO$ 1 and $Ginga$ spectra, exhibit a strong coupling between the photon index and the amount or reflection (see § 3.3), these results indicate the presence of a strong and variable reflection component. It should be noted that a time-resolved analysis of the $Ginga$ observation also suggested day-to-day variations in the amount of reflection component in IC 4329A (Fiore et al. 1992).

If the geometry of the AGN consists of a source illuminating hard X-rays above and below a soft X-ray–emitting disk (e.g., Haardt, Maraschi, & Ghisellini 1994), and these hard X-rays are produced by inverse Compton scattering of the soft X-rays, then the radiation field within the hard X-ray–emitting region is likely to be strongly anisotropic (Ghisellini et al. 1991). Therefore, the reflecting matter may see more radiation than that emitted toward the observer, by up to a factor of ~ 5, as a direct consequence of the electrons losing more energy in head-on collisions with the soft X-ray photons than in collisions from behind. In that case, a strong reflection component becomes physically plausible. However, anisotropy alone is unlikely to explain the increased contribution of the reflected component compared to that of the direct continuum, because it requires a change in the anisotropic factor. In other words, anisotropy can explain a high value of R but not a variation of R. Instead, a time-lag effect could, alone, explain all of the observational constraints. Although IC 4329A has never

exhibited strong, rapid variability, it has varied up to a factor of ~ 2.8 (from a 2–10 keV flux of $\sim 5 \times 10^{-11}$ ergs cm^{-2} s^{-1} to $\sim 14 \times 10^{-11}$ ergs cm^{-2} s^{-1}) on a timescale of ~ 5–6 yr, with a doubling timescale down to ~ 1 yr, in its ~ 20 yr history of X-ray observations. A time lag could therefore cause a strong amount of reflection. Our results can indeed be understood in this context if the continuum flux decreased by some amount prior to the $ASCA$ observation. Specifically, the flux would have to have decreased by a factor of ~ 2 from a time when it was higher than that measured by $Ginga$, and the reflection component could not have had time to respond to this decrease. This can simultaneously explain a high value of R, a variation of R, and a higher absolute amount of reflection as compared to $Ginga$.

However, another difficulty with the above results is that strong reflection should be accompanied, in most cases, by a strong iron line. We note that the reflected spectrum used in our fitting procedure (§ 3.2) is averaged over all viewing angles and has, accordingly, a slightly different shape than a face-on reflected spectrum. The best-fit amount of reflection $R \sim 3.3$ therefore corresponds to a (~ 1.33 times) lower value $R \sim 2.5$ for a face-on view (Ghisellini, Haardt, & Matt 1994; Magdziarz & Zdziarski 1995). As a rough estimate, assuming an Fe K line EW of ~ 140 eV in the case $R = 1$ for a cold face-on disk and an incident power-law spectrum with $\Gamma \sim 2.0$, we expect an EW of ~ 300 eV (George & Fabian 1991). The best-fit amount of reflection therefore requires ~ 3 times more line than observed (EW $\simeq 89 \pm 33$ eV). This difference may be reconciled by reducing the abundance of iron or increasing the abundance of the light metals (lighter than iron) (Reynolds, Fabian, & Inoue 1995). Alternatively, if the Fe K line arises in an ionized disk, its EW can be very low even in the presence of strong reflection, because of either resonant trapping of line photons or complete ionization of iron (Ross & Fabian 1993; Życki & Czerny 1994). Compared to the neutral case, the ionized disk has a lower opacity at lower energies. This might help to explain why the reflection shows up at such low (~ 5–6 keV) energies in this source. However, we show that the above constraints can be considerably reduced because the EW obtained with an accretion disk line model is significantly higher.

The parameters of the Fe K line obtained from the SIS spectral analysis are consistent with the line being redshifted by ~ 100 eV and slightly broad ($\sigma \sim 110$ eV). These support the idea that a fit of the line with a disk line model (Fabian et al. 1989) would be more appropriate than a Gaussian fit. A disk line model takes into account the effects of Doppler broadening and gravitational and transverse redshifts, in order to calculate the characteristic line profile. The resulting line profile is highly asymmetric and often "double-horned." A remarkable example of the applicability of this model to Seyfert 1 galaxies has come from $ASCA$ long observations of MCG -6-30-15 (Tanaka et al. 1995).

We attempted a fit of the SIS data with the "diskline" model available in the XSPEC program. This model calculates the intensity and profile of the line from a flat, optically thick accretion disk as calculated in Fabian et al. (1989). The details of the line depend on the inclination i of the disk, on the inner R_{in} and outer R_{out} disk radii, and on the line emissivity α (assumed to vary as $R^{-\alpha}$). Following Mushotzky et al. (1995), we fix $R_{in} = 3R_S$ and $R_{out} = 1000 R_S$, where R_S is the Schwarzschild radius of the black hole ($R_S \sim 3 \times 10^5 M/M_\odot$ cm, with M the mass of the black hole). The inclination of the disk, i, is

also fixed at 0 (face-on) to be consistent with our assumption of a face-on reflection component. The line energy is fixed at 6.3, which corresponds to the redshifted energy of a fluorescence Fe K line. Only the normalization of the line and its emissivity α are free to vary. The fit yields $\alpha \simeq 2.30 \pm 0.20$ and an EW of 188 ± 60 eV. If i is allowed to vary, we obtain an upper limit of $i \lesssim 25°$ which confirms a posteriori that the assumption of a disk face-on is substantially correct. In this case, the EW is enhanced to 213^{+76}_{-63} eV. These results are characteristic of a disk observed face-on, in which most of the fluorescence Fe K line is emitted within a few tens of Schwarzschild radii. As stated above, with the use of a disk line model, the Fe K EW is in rough agreement with the value expected from the reflection component.

Strictly speaking, if a disk line model is included, we should also take into account relativistic effects on the (continuum) reflection component in order to have a self-consistent model. This model is not available at the moment. This problem will be explored in a later paper. However, relativistic corrections should merely produce an energy shift and/or broadening of the reflection component. Therefore, we expect these should not significantly affect the above results.

It should be noted, however, that the velocity width (FWHM $\simeq 12,000 \pm 8500$ km s^{-1}) of the Fe K line is still consistent with an average derived FWHM of $\simeq 4070 \pm 30$ km s^{-1} for the strong Balmer lines (Hα, Hβ, and Hγ) which dominate the optical spectrum of IC 4329A. This suggests that the Fe K line might, alternatively, be produced from the broad-line region. One-sided beaming of the continuum emission and/or obscuration may be necessary, however, to explain the apparent redshift of the line.

5. CONCLUSIONS

To summarize, the present observation has revealed the following:

1. The apparent soft X-ray spectrum of IC 4329A is complex, with a predominant soft excess (compared to a simple absorbed power law) at $E \lesssim 0.8$ keV and deep absorption structures between ~ 0.8 and 1.2 keV. The unprecedentedly high (greater than 10 in every channel) signal-to-noise ratio of this observation allows us to discard, directly from the residuals, a blackbody emission model as an alternative explanation for the soft excess. Instead, the soft X-ray spectrum is best described by two absorption edges at $E \sim 0.70$ keV and $E \sim 0.84$ keV, consistent with absorption by O VI, O VII or N VII, and O VIII, respectively. This complex absorption is clearly the signature of a warm absorber, confirming and extending previous results obtained from *ROSAT* observations (Madejski et al. 1995).

2. It has confirmed the existence of a "hard tail" at higher energies, characteristic of a reflection component (Mushotzky et al. 1995). The hard tail is clearly detected in both the GIS and the SIS, at similar intensities. When the reflection is included, we find that the data prefer a stronger absolute amount of reflection and a stronger contribution relative to the direct continuum than previously observed. A time-lag effect can account for all observational constraints.

3. Because of the presence of the reflection component, the Fe K line width and EW are model dependent. These are, however, only weakly model dependent, provided R is higher than ~ 2.1 (§ 3.3). With the proposed best-fit model (with $R \simeq 3.3 \pm 1.1$), we find evidence that the Fe K line is redshifted (by ~ 100 eV) and slightly broad ($\sigma \simeq 0.11 \pm 0.08$ keV), as expected if the emission line is emitted by an accretion disk. The weak (EW $\simeq 89 \pm 33$ eV) Fe K (Gaussian) line requires iron underabundance and/or ionized matter to be consistent with strong reflection. A fit with a disk line model which includes the wings of the line can, however, account for most of the discrepancy as well.

REFERENCES

Arnaud, K. A., Haberl, F., & Tennant, A. 1991, XSPEC User's Guide (ESA TM-09)
Elvis, M., Lockman, F. J., & Wilkes, B. J. 1989, AJ, 97, 777
Fabian, A. C., Rees, M. J., Stella, L., & White, N. E. 1989, MNRAS, 238, 729
Fabian, A. C., et al. 1994, PASJ, 46, L59
Ferland, G. L. 1991, Ohio State Univ., Astron. Dept. Internal Rep. 91-01
Fiore, F., Perola, G. C., Matsuoka, M., Yamauchi, M., & Piro, L. 1992, A&A, 262, 37
George, I. M., & Fabian, A. C. 1991, MNRAS, 249, 352
George, I. M., Turner, T. J., & Netzer, H. 1995, ApJ, 438, L67
Ghisellini, G., George, I. M., Fabian, A. C., & Done, C. 1991, MNRAS, 248, 14
Ghisellini, G., Haardt, F., & Matt, G. 1994, MNRAS, 267, 743
Guainazzi, M., Matsuoka, M., Piro, L., Mihara, T., & Yamauchi, M. 1994, ApJ, 436, L35
Guainazzi, M., et al. 1995, PASJ, submitted
Guilbert, P. W., & Rees, M. J. 1988, MNRAS, 233, 475
Haardt, F., Maraschi, L., & Ghisellini, G. 1994, ApJ, 432, L95
Hayashida, K., et al. 1995, in preparation
Krolik, J. H., & Kriss, G. A. 1995, ApJ, 447, 512
Leighly, K., et al. 1995, ApJ, submitted
Lightman, A. P., & White, T. R. 1988, ApJ, 335, 57
Lotz, W. 1968, J. Opt. Soc. Am., 58, 915
Madejski, G. M., et al. 1995, ApJ, 438, 672
Magdziarz, P., & Zdziarski, A. A. 1995, MNRAS, 273, 837
Matsuoka, M. 1994, in New Horizon of X-Ray Astronomy, ed. F. Makino & T. Ohashi (Tokyo: Universal Academy Press), 305
Mihara, T., Matsuoka, M., Mushotzky, R. F., Kunieda, H., Otani, C., Miyamoto, S., & Yamauchi, M. 1994, PASJ, 46, L137

Miura, N., et al. 1995, in preparation
Miyoshi, S., et al. 1988, PASJ, 40, 127
Morrison, R., & McCammon, D. 1983, ApJ, 270, 119
Mushotzky, R. F., Fabian, A. C., Iwasawa, K., Kunieda, H., Matsuoka, M., Nandra, K., & Tanaka, Y. 1995, MNRAS, 272, L9
Nandra, K., & Pounds, K. A. 1994, MNRAS, 268, 405
Netzer, H. 1993, ApJ, 411, 594
Otani, C. 1995, Ph.D. thesis, Univ. Tokyo
Otani, C., & Dotani, T. 1994, ASCA News, 2, 25
Petre, R., Mushotzky, R. F., Krolik, J., & Holt, S. S. 1984, ApJ, 280, 499
Piro, L., Yamauchi, M., & Matsuoka, M. 1990, ApJ, 360, L35 (PYM90)
Ptak, A., Yaqoob, T., Serlemitsos, P. J., Mushotzky, R. F., & Otani, C. 1994, ApJ, 436, L31
Raymond, J. C., & Smith, B. W. 1977, ApJS, 35, 419
Reynolds, C. S., Fabian, A. C., & Inoue, H. 1995, MNRAS, in press
Ross, R. R., & Fabian, A. C. 1993, MNRAS, 261, 74
Tanaka, Y., Inoue, H., & Holt, S. S. 1994, PASJ, 46, 37
Tanaka, Y. et al. 1995, Nature, 375, 659
Turner, T. J., & Pounds, K. A. 1989, MNRAS, 240, 833
Turner, T. J., Weaver, K. A., Mushotzky, R. F., Holt, S. S., & Madejski, G. M. 1991, ApJ, 381, 85
Weaver, K. A., Arnaud, K. A., & Mushotzky, R. F. 1995, ApJ, 447, 121
Weaver, K. A., Nousek, J., Yaqoob, T., Hayashida, K., & Murakami, S. 1995, ApJ, 451, 147
Wilkes, B. J., & Elvis, M. 1987, ApJ, 323, 243
Wilson, A. S., & Penston, M. V. 1979, ApJ, 232, 389
Życki, P. T., & Czerny, B. 1994, MNRAS, 266, 653